Applied Catalysis B: Environmental 220 (2018) 626–634

Contents lists available at ScienceDirect

Applied Catalysis B: Environmental

journal homepage: www.elsevier.com/locate/apcatb

Research paper

Insights into perovskite-catalyzed peroxymonosulfate activation: Maneuverable cobalt sites for promoted evolution of sulfate radicals

Xiaoguang Duan[a,1], Chao Su[a,1], Jie Miao[b], Yijun Zhong[a], Zongping Shao[a,b,*], Shaobin Wang[a,*], Hongqi Sun[c]

[a] Department of Chemical Engineering, Curtin University, GPO Box U1987, WA, 6845, Australia
[b] State Key Laboratory of Materials-Oriented Chemical Engineering, Nanjing Tech University, No.5 Xin Mofan Road, Nanjing, 210009, PR China
[c] School of Engineering, Edith Cowan University, Joondalup, WA, 6027, Australia

ARTICLE INFO

Keywords:
Heterogeneous catalysis
Perovskite
Cobalt
Peroxymonosulfate
Sulfate radicals
Oxygen vacancy

ABSTRACT

Metal-based catalysis has significantly contributed to the chemical community especially in environmental science. However, the knowledge of cobalt-based perovskite for aqueous phase oxidation still remains equivocal and insufficient. In this study, we discovered that $Ba_{0.5}Sr_{0.5}Co_{0.8}Fe_{0.2}O_{3-\delta}$ (BSCF) perovskite was exclusively effective for peroxymonosulfate (PMS) activation to produce free radicals, whereas the BSCF was inert to activate peroxydisulfate (PDS) and hydrogen peroxide. The BSCF/PMS exhibited superior performance to the benchmark Co_3O_4 nanocrystals and other classical PMS activators such as α-MnO_2 and spinel $CoFe_2O_4$, meanwhile achieving an impressive stability with manipulated cobalt leaching in neutral and basic environment. *In situ* electron paramagnetic resonance (EPR) revealed the evolution of massive sulfate radicals ($SO_4\cdot^-$) and hydroxyl radicals (·OH) during the oxidation. A comprehensively comparative study of BSCF and Co_3O_4 nanocrystals was performed, including electrochemical impedance spectroscopy (EIS) and cyclic voltammograms (CV) in PMS solution as well as hydrogen temperature-programmed reduction (H_2-TPR) and oxygen temperature-programmed desorption (O_2-TPD) tests. The results unveil that the cobalt-based perovskite, BSCF, exhibited a better electrical conductivity and redox potential than the spinel cobalt oxide to interact with PMS. More importantly, the oxygen vacancies and less-electronegativity A-site metals may secure cobalt sites with a lower valence state for donating electrons to PMS simultaneously for radical generation. This study advances the mechanism of cobalt-based heterogeneous catalysis in environmental remediation.

1. Introduction

Sulfate radical ($SO_4\cdot^-$) based advanced oxidation processes (SR-AOPs) have aroused immense interests in environmental remediation in recent years. Sulfate radicals produced from persulfates exhibit several merits to hydroxyl radicals (·OH) from Fenton reactions, such as a higher oxidative capability (1.8-2.7 V NHE *vs* 2.5 V NHE of ·OH), a longer half-life period (30–40 μs *vs* 20 ns of ·OH), a better selectivity to target organics in complicated environment, and greater adaptive capability to a wide pH range from 2 to 8 (*vs* ~3.0 of Fenton reactions) [1–3]. Among persulfate salts, peroxymonosulfate (PMS) with an asymmetric structure ($HO-O-SO_3^-$) and a longer superoxide O—O bond (l_{O-O} = 1.326 Å) is believed more easily to be dissociated by a catalyst to generate $SO_4\cdot^-$ than peroxydisulfate (PDS), which possesses a symmetric structure ($^-_3OS-O-O-SO_3^-$) and a more compact O—O bond (l_{O-O} = 1.322 Å) [4,5].

Dionysiou and co-workers investigated a series of transition metals for generation of inorganic radicals from PMS and discovered that cobalt ions (Co^{2+}) were the most effective homogeneous catalysts for PMS activation [6,7]. Supported cobalt oxides on various other metal-oxide or carbon substrates were also developed as effective heterogeneous catalysts to minimize the toxic cobalt leaching and promote the dispersion of the cobalt oxide crystals [8–11]. Cobalt-containing spinel oxides such as $CoFe_2O_4$ and $CuCo_2O_4$ were also demonstrated to present a great activity for PMS activation owing to a synergistic effect of the redox couples between the different metal components [12–14]. More recently, Pang et al. applied $LaCoO_3$ perovskite to generate sulfate radicals from PMS for rapid mineralization of aqueous contaminants [15]. The La-based perovskites ($LaMO_3$, M = Co, Cu, Fe, and Ni) were further investigated and $LaCoO_3$ exhibited the best performance, confirming the critical role of cobalt in PMS activation [16].

In the heterogeneous cobalt-based catalysis, the catalytic activity of

* Corresponding authors at: Department of Chemical Engineering, Curtin University, GPO Box U1987, WA, 6845, Australia.
E-mail addresses: zongping.shao@curtin.edu.au (Z. Shao), shaobin.wang@curtin.edu.au, wang@exchange.curtin.edu.au (S. Wang).
[1] These authors contributed equally to this work.

http://dx.doi.org/10.1016/j.apcatb.2017.08.088
Received 3 March 2017; Received in revised form 21 June 2017; Accepted 30 August 2017
Available online 01 September 2017
0926-3373/ © 2017 Elsevier B.V. All rights reserved.

cobalt can be manipulated *via* several protocols. Firstly, the catalytic activity of cobalt oxide is intimately related with the surficial atom arrangement that governs the activation energy, kinetic behaviors, and electron-transport processes in binding with reactants and breaking the chemical bond in a catalytic reaction [17–20]. Thus, shape-controlled spinel Co_3O_4 could be synthesized by nano-engineering to predominantly expose certain crystal planes, which has been demonstrated as facet-dependent activity in methane combustion and carbon monoxide (CO) oxidation [21]. It is supposed that the [001] and [111] planes are mainly composed of Co^{2+}, which might present a better activity than other planes for PMS activation due to lower reductive potential of cobalt as an electron-donor. Secondly, supporting substrates would not only promote the dispersion of cobalt oxide with small particle sizes and high surface areas herein providing more active centers, but also impressively modulate the surface chemistry of the cobalt oxides *via* the covalent bonds between the catalysts and supports [22,23]. Studies have shown that the supports such as graphene [24], activated carbon fiber [25], and silicon oxide [26] could effectively enhance the activity of cobalt oxide for PMS activation. Moreover, substitutional doping other 3*d*-transition-metal cations into the tetrahedral site (Co^{2+}_{Td}) and octahedral site (Co^{3+}_{Oh}) of Co_3O_4 and rational design of mixed-metal spinel oxides such as $Co_{3-x}M_xO_4$ ($1 \leq \times \leq 2$, M = Zn, Ni, Fe, Mn) could further enhance the activity of cobalt, because the formation of Co−O−M bond could optimize the spinel structure and modulate the spin culture and electron localization of cobalt [27–29]. Meanwhile, the charge transfer from the redox couples between Co^{2+}/Co^{3+} and $M^{n+}/M^{(n+1)+}$ in the mixed metal oxides may further promote the catalytic activity for PMS activation as mentioned above.

Distinct from the mixed metal spinel oxides that could only be composed of several limited transition metal oxides to form a stable spinel structure, the perovskite oxides with a typical ABO_3 structure, where A sites are larger-sized alkali and rare earth metals and B sites are 3*d* transition metal ions, are capable of hosting more than 90% of metal elements in the periodic table [30,31]. More importantly, the structural, physicochemical and electronic properties of perovskites could be easily tuned by regulating the category and proportion of chemical compositions, providing a versatile substrate in the community of chemistry and materials science. Herein, the perovskites have attained great successes in a marriage of diverse catalytic progresses stretching from electrocatalysis to photocatalysis [32,33]. Nevertheless, several recent studies employed cobalt-based perovskites as persulfate activators to generate sulfate radicals, while the massive metal-leaching severely plagued these materials as environmentally-benign catalysts for green remediation due to the strong toxicity of cobalt [15,16,34,35]. Additionally, the mechanism of perovskite-catalyzed peroxymonosulfate still remains piecemeal and ambiguous, which requires an insightful study for the identification of the inherent active sites and unravelling the evolution of the reactive radicals. In this study, we utilized $Ba_{0.5}Sr_{0.5}Co_{0.8}Fe_{0.2}O_{3-\delta}$ (BSCF) perovskite as a model catalyst for mediating sulfate radicals by activating PMS. Various *in situ* characterizations and comprehensive comparison with the benchmark nanocrystals of cobalt oxide were conducted. The BSCF demonstrated greater electrical conductivity and redox potential than cobalt oxide nanocrystals to bond with PMS for charge transport, benefited from the surficial oxygen vacancies and less electronegative A-site metals. Meanwhile, the initially produced hydroxyl radicals were witnessed to play a crucial role for mediating sulfate radicals, which were further confirmed as the dominating reactive species. We dedicate this study to unveiling the evolution of free radicals from PMS with the perovskite and to probing the manipulated cobalt sites in mixed metal oxides for the heterogeneous catalysis.

2. Materials and methods

2.1. Chemicals and materials preparation

All the chemicals were purchased from Sigma-Aldrich, Australia and received without further purification. The perovskite oxides such as BSCF, $SrCo_{0.9}Ti_{0.1}O_{3-\delta}$ (SCT), $PrBaCo_2O_{5+\delta}$ (PBC) and $LaCoO_3$ were prepared *via* a classic sol–gel approach and calcination reported in our previous study [36]. In a typical process (*e.g.* BSCF), a stoichiometric dosage of metal nitrates such as $Ba(NO_3)_2$, $Sr(NO_3)_2$, $Co(NO_3)_2{\cdot}6H_2O$ and $Fe(NO_3)_3{\cdot}9H_2O$ with a molar ratio of 5:5:8:2 was first dissolved in deionized water to form a homogeneous solution at 100 °C. Ethylenediaminetetraacetic acid (EDTA) and citric acid (CA) were then introduced into the mixture solution at a molar ratio of 1:2:1 (EDTA:CA:total metal ions). The pH value of the solution was adjusted to around 6 with ammonium solution and heated at 100 °C to evaporate water and produce a transparent gel. The gel was pre-treated at 250 °C for 5 h and then calcined at 950 °C for 5 h in static air to be transformed into a uniformly mixed metal oxide with a characteristic perovskite crystal. SCT, PBC, and $LaCoO_3$ were obtained at 1000, 1000, and 800 °C, accordingly. The resulting products were ground finely for future use. The detailed preparation and structural information (Fig. S1) of other metal oxides such as cobalt oxide, manganese oxides, and spinel $CoFe_2O_4$ can be found in the Supplementary Data.

2.2. Characterization of perovskite

The morphologies of BSCF perovskite and spinel Co_3O_4 were revealed by a FESEM (Zeiss Neon 40EsB FIBSEM) in Fig. S2. The crystallographic structure of metal-based catalysts was determined by powder X-ray diffraction (XRD) on a Bruker D8A instrument. The XRD spectra were recorded with Cu-Kα radiation (λ = 1.78897 nm) within a two-theta range of 10–80° at a scanning speed of 2° min^{-1}. The specific surface areas (SSAs) and pore structure were acquired from a Micrometrics TriStar II equipment at −196 °C estimated by the Brunauer–Emmett–Teller (BET) and Barrett–Joyner–Halenda (BJH) equations, respectively. The redox potential of perovskite was evaluated by oxygen temperature-programmed desorption (O_2-TPD) and hydrogen temperature-programmed reduction (H_2-TPR). The O_2-TPD was performed from room temperature to 1000 °C under a constant argon flow. Oxygen was detected by an on-line mass spectrometer. The H_2-TPR was recorded on a ChemBET 3000 equipment. The sample was treated at 400 °C for 2 h under flowing N_2 to clean the surface contaminants and then reduced by 5% H_2 in N_2 at a flow rate of 90 mL min^{-1} and a ramping temperature of 5 °C min^{-1} from 35 to 1000 °C. The concentration of metal ions in the reaction solution was detected on a Perkin Optima 8300 ICP-OES. The surface elemental analysis was performed on an X-ray photoelectron spectroscopy (XPS, PHI 5000 VersaProbe) with an Al-Kα X-ray gun. The XPS spectra were analyzed with CasaXPS software using a Shirley background, and Voigt functions with a 30% Lorentzian component were applied for the component deconvolutions.

2.3. Catalytic evaluation of catalysts

The catalytic performance of the perovskites was evaluated for peroxymonosulfate activation and organic oxidation. The experiments were carried out in a batch reactor in a water bath maintained at 25 °C. The fixed amounts of PMS and catalyst were simultaneously introduced into the organic solution to initialize the oxidation; meanwhile mechanical stirring was kept to ensure a homogeneous solution throughout the reaction. Periodically, the mixture was withdrawn by a syringe and filtered *via* a 0.45 μm membrane, and the filtrate was mixed with methanol ($V_{filtration}$:$V_{methanol}$ = 2:1) to quench the reactive radicals and terminate the oxidation. The sample was then analyzed on a high-performance liquid chromatography (HPLC, Thermo-Fisher) using

an UltiMate™ 3000 RSLCnano System. The target organics were separated by an Acclaim organic acid LC column (150 × 4 mm, 5 μm) under a UV detector of 270 nm for phenol, nitrobenzene (NB), or hydroxybenzoic acid (HBA), and 228 nm for benzoic acid (BA). A pseudo-first-order kinetics was adopted for the estimation of initial reaction rate constants. The spent catalyst after each run was washed with water and ethanol several times and dried in an oven at 60 °C for stability tests. In the mechanistic study, the filtrate was directly mixed with 5, 5-dimethyl-1-pyrroline without quenching to trap the free radicals to form more stable adducts, which were further detected by the electron paramagnetic resonance (EPR). The sample was analyzed on the EPR under following parameter settings: center field = 3515 G, microwave frequency = 18.63 mW, attenuation = 10 dB, receiver gain = 30 dB, scan time = 30 s, and scan number = 2.

2.4. Electrochemical measurement

All the electrochemical measurements were conducted at room temperature in a standard three-electrode electrochemical cell with a Ag/AgCl (4 M KCl) reference electrode, a platinum wire counter electrode and a catalyst-modified glassy carbon working electrode (0.196 cm^2, Pine Research Instrumentation, USA), and the electrolyte was a mixture of 0.1 M Na_2SO_4 and 6.5 mM PMS. Homogeneous catalyst ink was first prepared by sonication of 10 mg catalyst powder, 10 mg conductive carbon (Super P, Alfa Aesar), 0.1 mL Nafion solution (5 wt%, Sigma-Aldrich) and 1 mL absolute ethanol. Then, 7 μL of the as-prepared catalyst ink was pipetted onto the surface of the glassy carbon electrode, leading to a catalyst loading of ~0.325 mg cm^{-2}. The catalyst layer was dried in ambient air before use. All the electrochemical data were collected on a CHI 760E bipotentiostat. Cyclic voltammetry (CV) measurement was conducted between −0.6–1.0 V *vs.* Ag/AgCl at a scan rate of 50 mV s^{-1}. Electrochemical impedance spectra (EIS) were recorded at −0.3 V *vs.* Ag/AgCl within a frequency range from 10^5 to 10^{-1} Hz using an AC voltage at a 5 mV amplitude.

3. Results and discussion

3.1. The catalytic activity of perovskite for superoxide activation

As illustrated in Fig. 1a, BSCF perovskite was employed for the activation of diverse superoxides such as H_2O_2, PMS, and PDS. Interestingly, the BSCF can effectively activate PMS for complete phenol degradation. However, negligible phenol removal was achieved in BSCF/PDS and BSCF/H_2O_2 systems, suggesting that the BSCF was not able to activate H_2O_2 and PDS to generate reactive species. Similar scenarios were also found for other perovskites of $LaCoO_3$-, SCT-, and PBC-based systems as shown in Figs. S3-S5. Therefore, the cobalt-based perovskite was revealed to be exclusively effective for peroxymonosulfate activation. Hereafter, we applied BSCF, one of the most classical perovskites, for the subsequent kinetic and mechanistic studies.

The performance of BSCF was also compared with three most popular PMS activators, α-MnO_2, spinel Co_3O_4, and $CoFe_2O_4$ (Fig. 1b), which have been well reported in previous studies [26,37,38]. Compared with 100% phenol oxidation in less than 30 min achieved on BSCF, $CoFeO_4$, Co_3O_4, and α-MnO_2 attained 19.9%, 60.7%, and 60.3% phenol removal in 60 min, respectively. The perovskite BSCF demonstrated the best activity among the effective transition metal oxides. The effects of catalyst, phenol, and PMS amounts were also investigated. The phenol removal rate significantly decreased while adding more phenol into the system due to the competitive reactions between free radicals and target organics (Fig. S6). However, the increase of the catalyst loading (Fig. S7) and PMS dosage (Fig. S8) would either introduce more active sites or generate more reactive radicals, giving rise to promoted efficiency in phenol decomposition.

3.2. Identification of the reactive species in perovskite catalyzed PMS activation

Since peroxymonosulfate, with an asymmetric structure (HO−O−SO_3^-), can be activated to produce either hydroxyl radicals *via* Eq. (1) or sulfate radicals *via* Eq. (2), meanwhile the radicals would undergo mutual transformation *via* Eqs. (3) and (4) which were partially manipulated by solution pH. To further probe the principal reactive species accounting for the organic oxidation, selective radical quenching tests were performed with *tert*-butyl alcohol (TBA) and methanol (MeOH). Methanol, with three α-H connected to the carbon atom adjacent to the hydroxyl group ((α-H)$_3$−C−OH), can readily react with both $SO_4^{\cdot-}$ and ·OH in high reaction rates ($k_{SO4^{\cdot-}}$ = (1.6–7.7) × 10^7 M^{-1} s^{-1}, $k_{\cdot OH}$ = (1.2–2.8) × 10^9 M^{-1} s^{-1}), whereas, TBA ((CH$_3$)$_3$−C−OH) without α-H presents a much higher reaction rate with ·OH ($k_{SO4^{\cdot-}}$ = ($k_{\cdot OH}$ = (3.8–7.6) × 10^8 M^{-1} s^{-1}) than $SO_4^{\cdot-}$ ($k_{SO4^{\cdot-}}$ = (4.0-9.1) × 10^5 M^{-1} s^{-1}) [39]. As shown in Fig. 2a, the addition of radical quenching agents dramatically slowed down the phenol oxidation, suggesting that the perovskite/PMS is a radical-dominated system, which is intrinsically different from our recent discovery of nanocarbon/PMS with a nonradical pathway that the alcohols could hardly impede the oxidation [5,40]. More specifically, 53.8 and 36.9% of phenol oxidation efficiencies were achieved when 200 and 500 times of molar-ratio of TBA/PMS were presented, in contrast to 100% organic removal during 60 min in the controlled experiment without any radical scavengers. Inferior oxidative efficiencies of 24.3

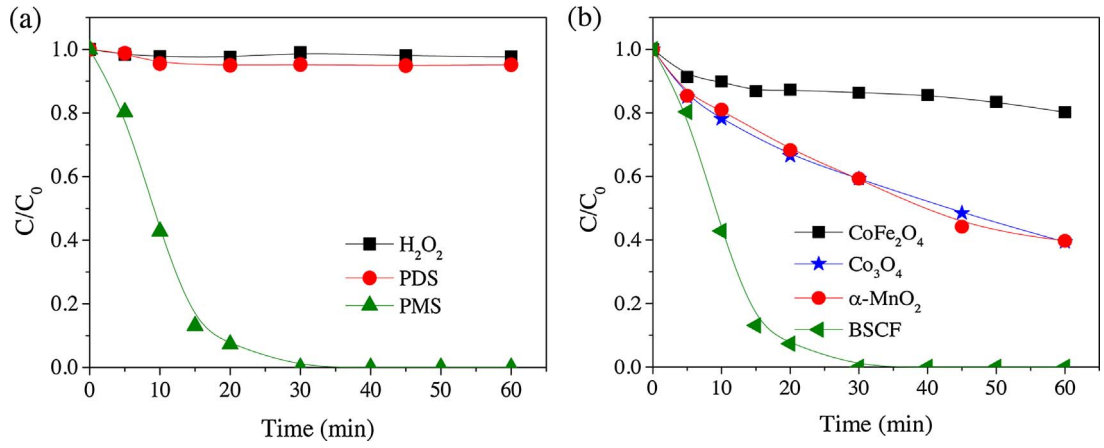

Fig. 1. (a) Catalytic activation of different superoxides by BSCF ([catalyst] = 0.1 g L^{-1}, [phenol] = 20 mg L^{-1}, [PMS] = [PDS] = [H_2O_2] = 6.5 mM); (b) Comparison of different metal-based catalysts for phenol catalytic oxidation with PMS ([PMS] = 6.5 mM).

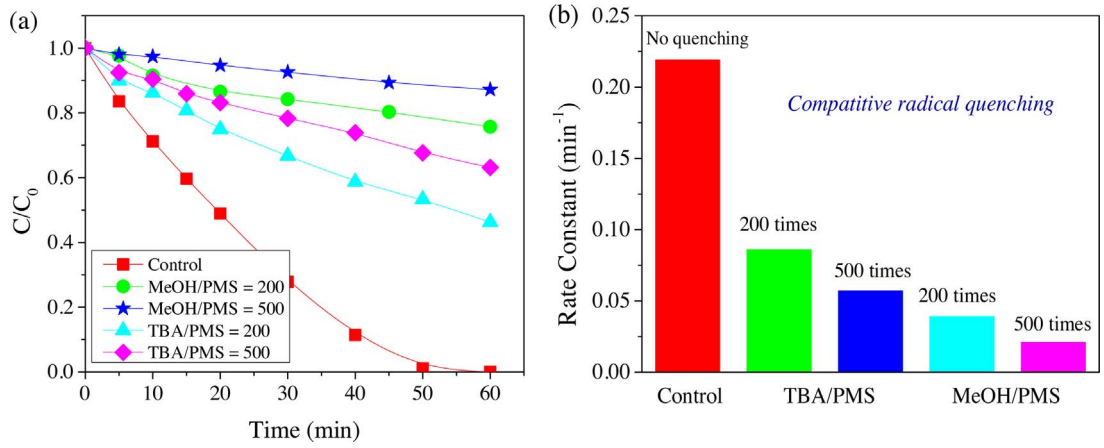

Fig. 2. Competitive radical quenching tests (a) and initial reaction rate constants (b) of BSCF-catalyzed PMS activation ([catalyst] = 0.1 g L^{-1}, [phenol] = 40 mg L^{-1}, [PMS] = 6.5 mM).

and 12.8% phenol degradation were attained in the presence of 200 and 500 times higher of methanol to PMS, respectively. The initial rate constants in Fig. 2b illustrates that both sulfate and hydroxyl radicals were accounted for organic mineralization, and the lower rate constants with MeOH imply that the sulfate radicals might play a more crucial role in phenol decomposition. The perovskite-based system was also effective for the degradation of other organic contaminants (Fig. S9). A complete oxidation of hydroxyl benzoic acid (HBA) was attained in BSCF/PMS as well as 55.7 and 30.0% degradation of nitrogen benzene (NB) and benzoic acid (BA) accordingly. It is worth noting that both NB and BA are only sensitive to hydroxyl radicals and reluctant to sulfate radicals. Hence, the distinct oxidative performances for the different organics further verified the existence of ·OH and the dominant role of SO_4·$^-$.

$$HSO_5^- + Me^{n+} \rightarrow {}^{\circ}OH + SO_4^{2-} + Me^{(n+1)+} \quad (1)$$

$$HSO_5^- + Me^{n+} \rightarrow SO^{\circ}{}_4 + OH^- + Me^{(n+1)+} \quad (2)$$

$$^{\circ}OH + SO_4^{2-} \rightarrow SO^{\circ-}_4 + OH^- \quad (3)$$

$$SO^{\circ-}_4 + OH^- \rightarrow SO_4^{2-} + {}^{\circ}OH \quad (4)$$

$$HSO_5^- + {}^{\circ}OH \rightarrow SO^{\circ-}_4 + O_2^{2-} + 2H^+ \quad (5)$$

$$HSO_5^- + Me^{(n+1)+} \rightarrow SO^{\circ-}_4 + OH^- + Me^{n+1} \quad (6)$$

Electron paramagnetic resonance (EPR) technology has been demonstrated as a powerful tool to *in situ* detect the free radicals in an aquatic system. In this study, 5, 5-dimethyl-1-pyrroline (DMPO) was utilized as a spin trapping agent to capture the reactive intermediates during PMS activation. As shown in Fig. 3a and Fig. S10, the EPR spectra clearly evidenced the characteristic peaks for DMPO—OH adducts (α_H = 14.8, α_N = 14.8) and DMPO-SO_4 (α_H = 0.78, α_H = 1.48, α_H = 9.6, and α_N = 13.2). Fig. 3b witnessed a rapid generation of massive hydroxyl radicals in the first 10 min and a slower increasing rate afterward. However, the circumstances for sulfate radicals are different. The peak density of DMPO-SO_4 impressively enhanced in the first 20 min, and then decreased for the continuing oxidation. It should be pointed out that the initial intensity of DMPO—OH was much higher than DMPO-SO_4 in the first few minutes. Since the pH of reaction solution would be rapidly acidified (from ~6 to ~3) due to the addition of PMS (HSO_5^-) and formation of mineralized by-products, the transition from ·OH to SO_4·$^-$ *via* Eq. (3) should be suppressed. We assume that the premier ·OH may react with PMS and promote the generation of SO_4·$^-$ *via* Eq. (5). A similar phenomenon was also unveiled in Huang's study that the hydroxyl radical was first produced in ACFs-CoPc/PMS (cobalt phthalocyanine anchored onto activated carbon fibers) and continuously activate PMS to generate sulfate radicals [25]. The DMPO-SO_4 declined after 20 min due to the consumption of sulfate radicals during continuous organic oxidation. A proposed reaction mechanism is displayed in Fig. 4 that PMS was activated by BSCF to generate both sulfate and hydroxyl radicals for phenol degradation into harmless carbon dioxide and water.

3.3. Impact of solution pH and metal leaching

In the advanced oxidative processes, the solution pH would dramatically influence the oxidative effectiveness of the PMS-based system

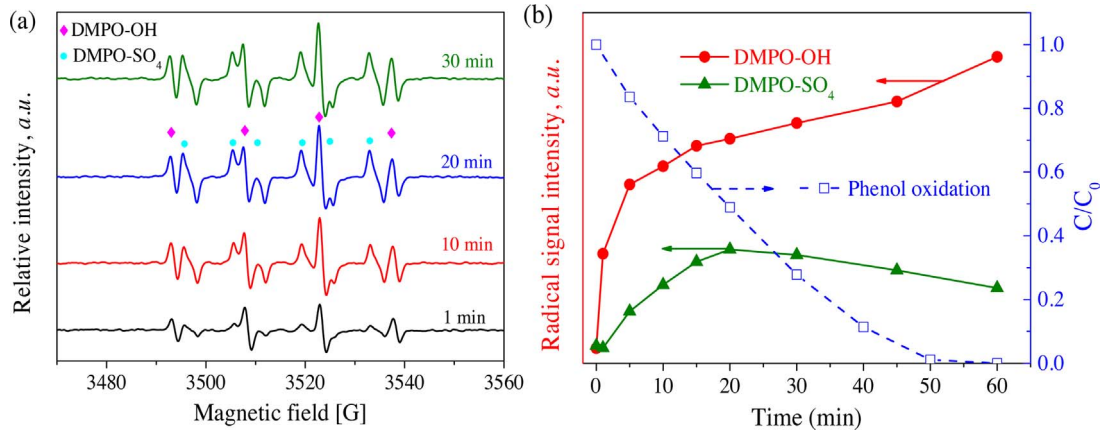

Fig. 3. EPR spectra (a) and radical evolution (b) of BSCF/PMS system for phenol degradation ([catalyst] = 0.1 g L^{-1}, [phenol] = 40 mg L^{-1}, [PMS] = 6.5 mM, and [DMPO] = 0.8 M).

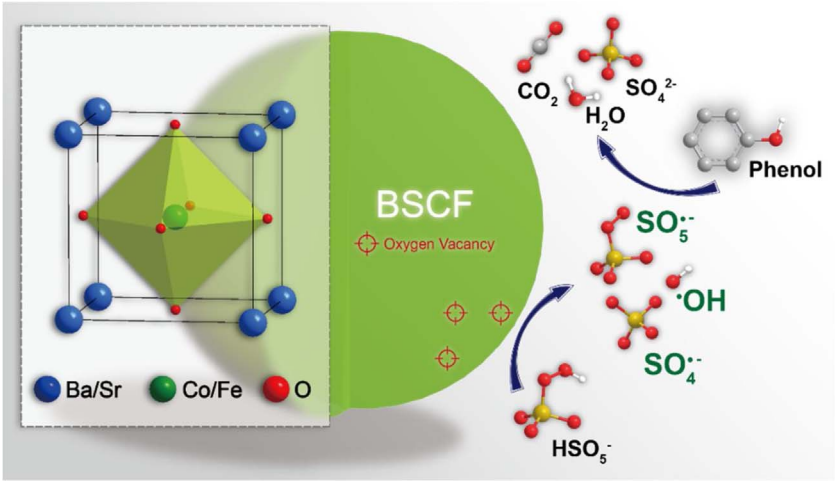

Fig. 4. A proposed mechanism of BSCF-catalyzed PMS activation.

in several aspects. Firstly, the pH can affect the forms of PMS molecules ($pK_{a1} < 0$; $pK_{a2} = 9.88$), herein impacting the reactivity of the PMS with the catalyst [41]. The basic ion of PMS ($^{-}O{-}O{-}SO_3^{-}$) in alkane condition presents a higher oxidative potential than its parent acid (H_2SO_5) and is able to be activated by the base to generate sulfate and hydroxyl radicals [42,43]. Secondly, the pH can alter the molecular structure of the target organics and mineralized intermediates. Since phenol exists as phenolate ($^{-}O{-}C_6H_5$) in basic condition, the electron-donating oxygen groups with bare electrons would donate charges to the benzene ring with a denser charge density, which would facilitate the addition and H abstraction reactions with the electron-affinity free radicals. Thirdly, solution pH can manipulate the radical species in AOPs. It has been well reported that sulfate radical-based reaction would be transferred into hydroxyl radical-based systems under alkaline condition due to the interconvertible manner of the free radicals *via* Eqs. (3) and (4) [44,45]. Moreover, the pH would alter the surface property of metal oxides. As the surface of metal oxides is functionalized with hydroxyl radicals in the aqueous phase, and the acidity/alkalinity and surface charge property could be regulated by the solution pH, which then influences the adsorption and binding capability with the reactants in the heterogeneous reaction [46]. Additionally, the pH would affect the leaching of metal oxides in water as the acidic environment leads to the corrosion of metal surface and destruction of the crystal structure, giving rise to heavy leaching of toxic metal ions and inferior stability for multiple usages.

The effects of solution pH were then investigated in the BSCF/PMS system. Not surprisingly, as illustrated in Figs. 5 a, b and S11, phenol removal efficiency and rate constants were promoted with the elevated initial pH from 2.5 to 8.0. The BSCF perovskite exhibited a better activity than the benchmark spinel Co_3O_4 in a wide pH range. More importantly, the cobalt leaching was controlled from 5.90 mg L^{-1} ($pH_{initial}$ = 2.5) to 3.61 mg L^{-1} ($pH_{initial}$ = 8.0), which is even lower than that of Co_3O_4 (5.87 mg L^{-1}, $pH_{initial}$ = 5.6). The buffer solution was also evaluated as shown in Figs. 5 c, d and S12. Despite the fact that the buffer agents may partially screen the reactive radicals, the buffered system can still achieve a high phenol oxidation and total organic carbon (TOC) removal (inset of Fig. 5c) in the basic condition. More importantly, the cobalt-leaching was dramatically suppressed when the solution was buffered to 8.0. Only 0.75 mg L^{-1} (Co^{2+}) was detected compared with the unbuffered solution with 5.87 mg L^{-1} (Co^{2+}). Without a buffer solution, the reaction solution would be changed to pH = 3.5 after PMS addition. In addition, the pH of solution was further reduced due to intermediate weak acids generated during the reaction. At controlled pH 8, the basic condition is beneficial to protecting the surface crystallinity of the perovskite and effectively preventing the metal leaching into the reaction solution. Therefore, the metal leaching of the perovskite-based system can be effectively alleviated by adjusting the solution to a moderate or slightly alkaline environment, meanwhile maintaining the higher catalytic performance of the catalyst. However, a highly basic condition may not be favorable, otherwise, the base activation would take effects. In addition, base activation requires intensive extra chemical inputs of the base, and produces hydroxyl radicals and singlet oxygen instead with lower redox potential than the sulfate radicals [42]. Guan et al. reported PMS would exsit in the form of SO_5^{2-} when pH is over 9, which prevented the interaction between PMS and metal oxide surface ($\equiv MOH \rightarrow \equiv MO-$) through the strong electrostatic repelling force between the negatively-charged reactant and catalyst, herein slowing down the PMS activation and organic degradation significantly [47].

3.4. Stability of BSCF for phenol oxidation

The reusability of the perovskite was also evaluated. As displayed in Fig. 6a, BSCF exhibited an excellent stability with a complete phenol oxidation in 30 min for the fresh catalyst, and 40 and 60 min for the 2nd and 3rd cycles accordingly. The stability of BSCF for multiple runs could be comparable to the effective PMS activators of metal oxides such as α-MnO_2 [38], Co_3O_4 [48], $CoFe_2O_4$ [49], and $CuFe_2O_4$ [14]. The XRD spectra in Fig. 6b confirmed that the spent BSCF maintained the robust perovskite structure without phase transition, and the minor unknown phases might be attributed to the formation of insoluble sulfate and carbonate contaminants, which partially covered the active sites on the BSCF surface and resulted in the deactivation of the catalyst. Fig. 6c displayed the high resolution XPS spectra of Co 2p core-level. Because of the severe overlap of Co 2p and Ba 3d in XPS spectra, it is hard to precisely reveal the cobalt states by peak fitting [50,51]. However, the two main peaks obviously shifted to the higher binding energies for the spent catalysts, implying that the valence state of cobalt increased from Co^{2+} to Co^{3+} due to transferring electrons to PMS to generate sulfate radicals. The XPS spectra of O 1s core levels of BSCF in Fig. 6d could be deconvoluted into four peaks located at 527.7, 529.7, 530.9, 532.1 eV, accordingly, representing the lattice oxidation ions (O^{2-}), less electron-rich oxygen species (O_2^{2-}/O^{-}), hydroxyl groups, and adsorbed molecular water, respectively [52]. The percentage of surface lattice oxygen ions slightly decreased after the reaction, possibly ascribed to the surface destruction from leaching and the formation of contaminants as illustrated in the XRD spectra.

3.5. Mechanism of promoted PMS activation by cobalt-based perovskite

In this study, the cobalt-based perovskites demonstrated superb catalytic activities than the benchmark spinel Co_3O_4 nanocrystals.

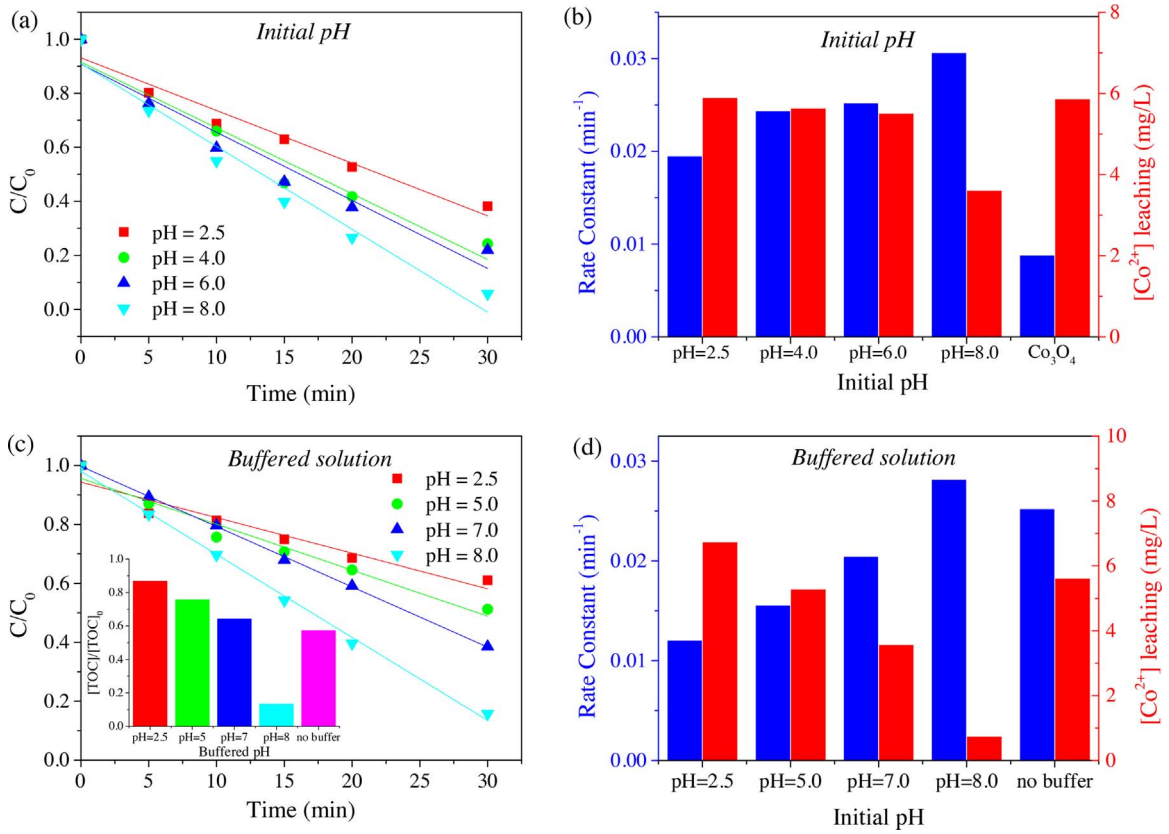

Fig. 5. Effects of initial pH (a) (b) and buffered pH (c) (d) in BSCF/PMS system ([catalyst] = 0.1 g L^{-1}, [phenol] = 40 mg L^{-1}, [PMS] = 6.5 mM).

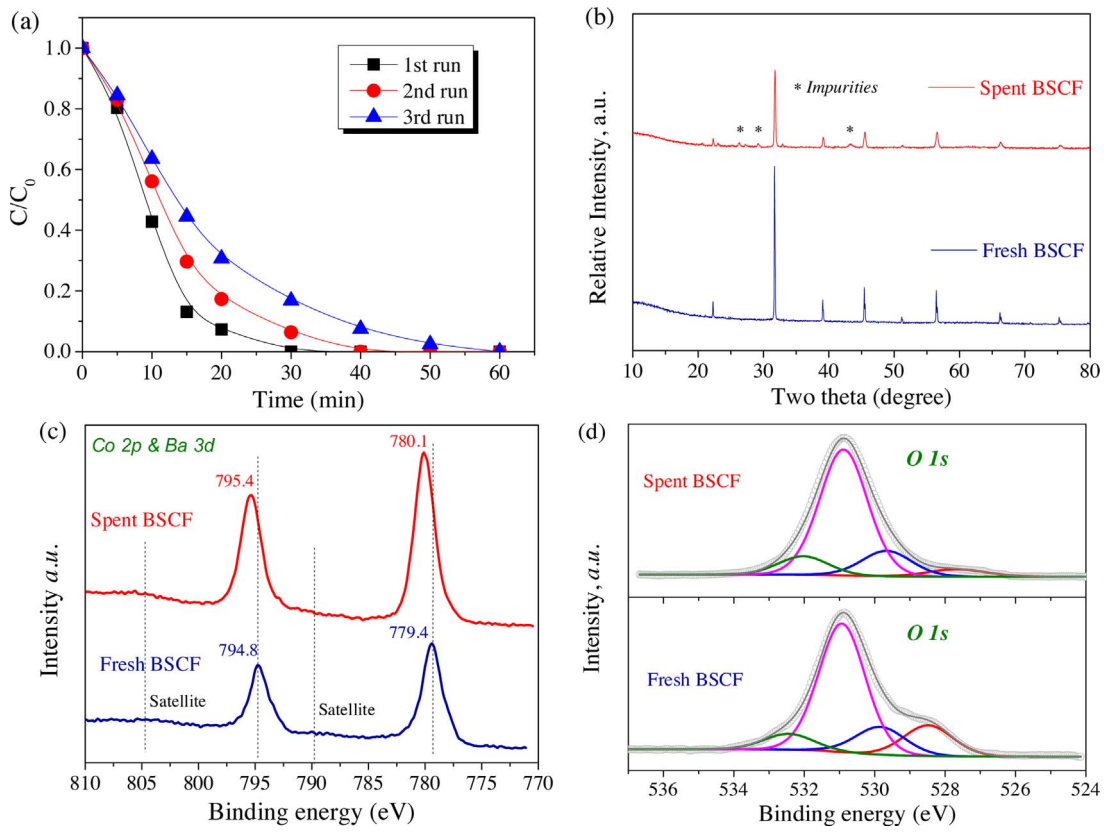

Fig. 6. (a) Stability tests of BSCF in unbuffered solution ([catalyst] = 0.1 g L^{-1}, [phenol] = 40 mg L^{-1}, [PMS] = 6.5 mM, [DMPO] = 0.8 M); (b) XRD profiles, and high resolution XPS spectra of Co 1s (c) and O 1s (d) of fresh and spent BSCF catalysts.

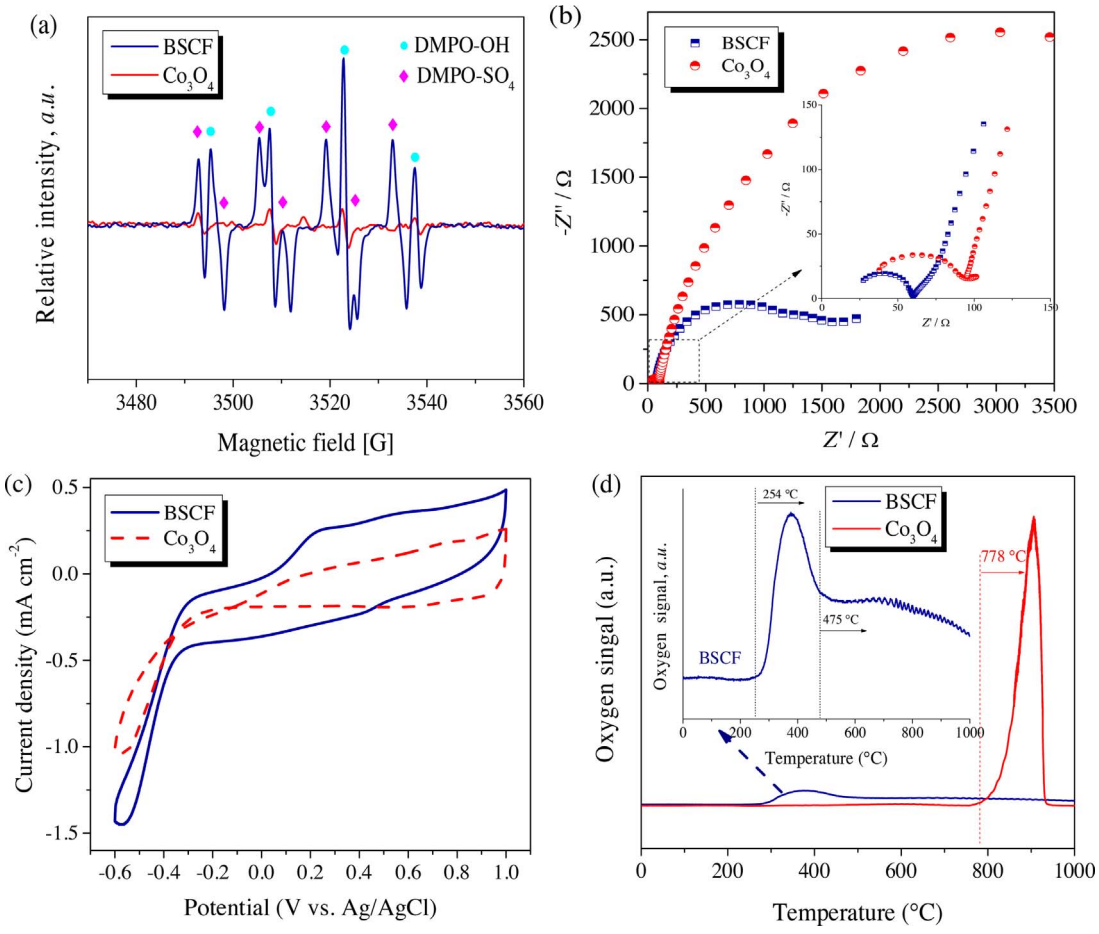

Fig. 7. Comparison of the BSCF perovskite and spinel Co_3O_4 nanocrystal for (a) EPR spectra ([catalyst] = 0.1 g L^{-1}, [phenol] = 40 mg L^{-1}, [PMS] = 6.5 mM, [DMPO] = 0.8 M), (b) EIS Nyquist plots collected at −0.3 V *vs.* Ag/AgCl, (c) CV curves at a scan rate of 50 mV s^{-1}, and (d) O_2-TPD profiles.

Nevertheless, the bulk BSCF catalyst only possesses an SSA of 0.43 m^2 g^{-1} *vs.* Co_3O_4 of 35.3 m^2 g^{-1}, the turnover frequencies (TOF) of BSCF and Co_3O_4 for phenol conversion were estimated to be 0.109 and 0.00134 s^{-1}, respectively. The TOF of BSCF was 81.4-fold higher than that of the spinel Co_3O_4. The EPR spectra in Fig. 7a demonstrate that BSCF exhibited stronger intensities of DMPO−OH and DMPO-SO_4 adducts than Co_3O_4, implying that the BSCF can effectively activate PMS to generate more sulfate and hydroxyl radicals, which resulted in the extraordinary performance of the perovskite for phenol oxidation.

The electrochemical evaluation was performed to probe the charge-transfer capacity and redox potential of catalysts in PMS solution. As illustrated in Fig. 7b, BSCF presented a smaller semicircle than that of Co_3O_4 within a high-frequency region in the EIS Nyquist plots, suggesting that the BSCF perovskite exhibited a better electric conductivity in the heterogeneous reaction, which is beneficial to the charge transfer for PMS activation [53,54]. The CV curves in Fig. 7c also indicate that BSCF presented a higher current density and greater reductive capability than Co_3O_4 to coordinate a redox process. The mild peaks at 0.21 and 0.54 V could be assigned to the redox couples of Co^{2+}/Co^{3+} and Co^{3+}/Co^{4+} accordingly due to the valence-state transfer of cobalt sites as $Co(OH)_2$(II) ↔ CoOOH(III) ↔ CoO_2(IV) in BSCF [37,54]. The oxygen mobility and redox ability of BSCF and Co_3O_4 were further investigated by O_2-TPD. The peak in the O_2-TPD profiles is an apparent indicator for the change of oxidative states of cobalt-ions. Metal oxides would undergo a thermal reduction from high to low valence states at elevated temperature whilst releasing oxygen and harvesting oxygen vacancies (for perovskite) [55]. As shown in Fig. 7d, the BSCF catalyst displayed two-stage desorption processes initialized at around 254 °C followed by a broad peak at 475 °C, which could be accounted for $Co^{4+} \rightarrow Co^{3+}$ and $Co^{3+}/Fe^{3+} \rightarrow Co^{2+}/Fe^{2+}$, respectively. However, the O_2 only started to be released at a higher temperature of 778 °C for Co_3O_4. It suggests that the cobalt-ions with unique transitive states in BSCF may provide better redox potential for a catalytic reaction, which could be further supported by H_2-TPR in Fig. S13.

As illustrated in Fig. 8, the BSCF in this study is composed of cubic units with lattice parameters of $a = b = c = 3.986$ Å. The Co/Fe cations in the B-site are trapped in the center of the cube and the A-site cations (Ba/Sr) are located at the corners of the cubic cells. However, the Co_3O_4 nanocrystals are constructed with a typical spinel structure with one Co(II) cation in the tetrahedral center and two Co(III) cations at the octahedral site within a pseudocubic unit of $a = b = c = 8.080$ Å. Thus, BSCF possesses a more uniform structure that may facilitate the charge transport within the perovskite. Additionally, despite the fact that the rare-earth metals in the A-site are reported to be chemically inert, introducing Ba into the A-site would enhance the phase stability, synergistically promote the catalytic activity of B-site, and maintain a high level of oxygen vacancies during the high-temperature annealing synthesis [55,56]. The spin culture and oxidation state of cobalt and oxygen defective level could be effectively governed by simply harnessing the category and nature of A-site [31]. Furthermore, the Ba ($\chi = 0.9$) and Sr ($\chi = 1.0$) in the A-site possess a lower electronegativity than Co ($\chi = 1.9$), which leads to a denser electron population of the cobalt and facilitates the charge transfer between PMS and the catalyst to produce sulfate radicals. Besides, the surface oxygen vacancies might promote the binding with water molecules to form hydroxyl groups, which would interact with the oxidant and enable electron transport from Co^{2+}/Co^{3+} to PMS *via* the hydroxyl bonding (BSCF−Co(II)−OH−HO−SO_3) to break the O−O bond of PMS

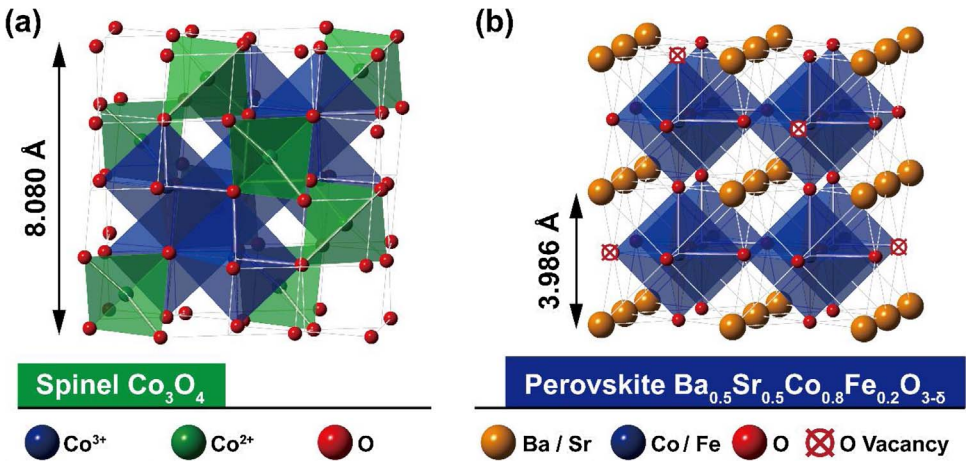

Fig. 8. Crystal structures of (a) spinel-type Co_3O_4 and (b) perovskite-type BSCF.

[37]. Han et al. reported that the oxygen defects in perovskite could decrease the chemical valence of B-site metal ions [57]. Herein, the abundant oxygen vacancies in BSCF could afford a lower oxidation state of cobalt with greater tendency to donate electrons to PMS for radical generation and recovery of oxidized cobalt sites from Co^{3+} to Co^{2+} Eq. (6). Meanwhile, the unique presence of high-valence state Co^{4+} in BSCF expresses high redox potential (reflected in the CV curves and O_2-TPD), being able to react with PMS (HSO_5^-) to generate persulfate radicals ($SO_5\cdot^-$) and fulfill the redox cycle of Co^{4+}/Co^{3+}. Nevertheless, BSCF is a typical mixed ion-electronic conductor with outstanding oxygen permeability at high temperatures, thus is extensively applied as the cathode material in solid oxide fuel cells and the oxygen separation membrane [55,58]. The immigration of oxygen vacancies from an inner core to the outer sphere may be insignificant under atmospheric ambience in aqueous phase [58–61]. Thus, the exchange of oxygen-vacancies in the surface region or subsurface layer of BSCF might primarily play a key role due to the high charge and oxygen-ion conductivity, which would replenish the surface oxygen vacancies in tuning the surface cobalt oxidation state and participating in the PMS activation.

4. Conclusions

In summary, we applied cobalt-based perovskites as novel catalysts for PMS activation and generation of highly oxidative species. The BSCF/PMS demonstrated a superior activity to the popular metal oxides, and exhibited a great efficiency in the degradation of a wide range of contaminants. Besides, the BSCF perovskite manifested a good stability for multiple runs and a controllable manner of metal leaching, especially in neutral and slightly basic conditions. More importantly, selective radical quenching tests and *in situ* EPR unravelled that both hydroxyl and sulfate radicals were generated during PMS activation by BSCF. The initially generated hydroxyl radicals may contribute to the PMS decomposition and sulfate radicals played the dominant role in organic mineralization. The electrochemical measurement, H_2−TPR, and O_2−TPD revealed that the BSCF perovskite expressed a better electrical conductivity, an easier transition of cobalt valence states, and a greater potential than those of spinel cobalt oxide to mediate a redox process with PMS *via* a rapid charge transfer process. Moreover, the oxygen vacancies and A-site metal ions with a less electronegativity may afford cobalt sites with a high charge density in the cubic structure for interacting with PMS to produce free radicals. This study deepens the understanding of perovskite-catalyzed peroxymonosulfate activation in environmental remediation and advances the cobalt-based perovskite oxides in heterogeneous catalysis.

Acknowledgement

The authors acknowledge the financial supports from Australian Research Council under discovery projects of DP150103026 and DP170104264.

Appendix A. Supplementary data

Supplementary data associated with this article can be found, in the online version, at http://dx.doi.org/10.1016/j.apcatb.2017.08.088.

References

[1] W.D. Oh, Z.L. Dong, T.T. Lim, Appl. Catal. B 194 (2016) 169–201.
[2] P.D. Hu, M.C. Long, Appl. Catal. B 181 (2016) 103–117.
[3] F. Ghanbari, M. Moradi, J. Chem. Eng. 310 (2017) 41–62.
[4] H.Q. Sun, C. Kwan, A. Suvorova, H.M. Ang, M.O. Tade, S.B. Wang, Appl. Catal. B 154 (2014) 134–141.
[5] X.G. Duan, Z.M. Ao, H.Q. Sun, L. Zhou, G.X. Wang, S.B. Wang, Chem. Commun. 51 (2015) 15249–15252.
[6] G.P. Anipsitakis, D.D. Dionysiou, Environ. Sci. Technol. 38 (2004) 3705–3712.
[7] G.P. Anipsitakis, D.D. Dionysiou, Environ. Sci. Technol. 37 (2003) 4790–4797.
[8] P.R. Shukla, S.B. Wang, H.Q. Sun, H.M. Ang, M. Tade, Appl. Catal. B 100 (2010) 529–534.
[9] P.H. Shi, R.J. Su, S.B. Zhu, M.C. Zhu, D.X. Li, S.H. Xu, J. Hazard. Mater. 229 (2012) 331–339.
[10] W. Zhang, H.L. Tay, S.S. Lim, Y.S. Wang, Z.Y. Zhong, R. Xu, Appl. Catal. B 95 (2010) 93–99.
[11] Q.J. Yang, H. Choi, Y.J. Chen, D.D. Dionysiou, Appl. Catal. B 77 (2008) 300–307.
[12] Y. Feng, J.H. Liu, D.L. Wu, Z.Y. Zhou, Y. Deng, T. Zhang, K.M. Shih, J. Chem. Eng. 280 (2015) 514–524.
[13] Q. Yang, H. Choi, S.R. Al-Abed, D.D. Dionysiou, Appl. Catal. B 88 (2009) 462–469.
[14] T. Zhang, H.B. Zhu, J.P. Croue, Environ. Sci. Technol. 47 (2013) 2784–2791.
[15] X.T. Pang, Y. Guo, Y.T. Zhang, B.B. Xu, F. Qi, J. Chem. Eng. 304 (2016) 897–907.
[16] K.-Y.A. Lin, Y.-C. Chen, Y.-F. Lin, Chem. Eng. Sci. 160 (2017) 96–105.
[17] H.Q. Sun, H.M. Ang, M.O. Tade, S.B. Wang, J. Mater. Chem. A 1 (2013) 14427–14442.
[18] R. Narayanan, M.A. El-Sayed, Nano Lett. 4 (2004) 1343–1348.
[19] K.M. Bratlie, H. Lee, K. Komvopoulos, P.D. Yang, G.A. Somorjai, Nano Lett. 7 (2007) 3097–3101.
[20] L. Zhang, W.X. Niu, G.B. Xu, Nano Today 7 (2012) 586–605.
[21] K.B. Zhou, Y.D. Li, Angew. Chem. Int. Ed. 51 (2012) 602–613.
[22] D.Y. Wang, M. Gong, H.L. Chou, C.J. Pan, H.A. Chen, Y.P. Wu, M.C. Lin, M.Y. Guan, J. Yang, C.W. Chen, Y.L. Wang, B.J. Hwang, C.C. Chen, H.J. Dai, J. Am. Chem. Soc. 137 (2015) 1587–1592.
[23] C. Jiang, C.P. Yuan, P.H. Li, H.G. Wang, Y.H. Li, Q. Duan, J. Mater. Chem. A 4 (2016) 7251–7256.
[24] Y.J. Yao, Z.H. Yang, H.Q. Sun, S.B. Wang, Ind. Eng. Chem. Res. 51 (2012) 14958–14965.
[25] Z.F. Huang, H.W. Bao, Y.Y. Yao, W.Y. Lu, W.X. Chen, Appl. Catal. B 154 (2014) 36–43.
[26] P. Shukla, H.Q. Sun, S.B. Wang, H.M. Ang, M.O. Tade, Sep. Purif. Technol. 77 (2011) 230–236.
[27] M.J. Zhou, L.L. Cai, M. Bajdich, M. Garcia-Melchor, H. Li, J.J. He, J. Wilcox, W.D. Wu, A. Vojvodic, X.L. Zheng, ACS Catal. 5 (2015) 4485–4491.
[28] H.Y. Wang, S.F. Hung, H.Y. Chen, T.S. Chan, H.M. Chen, B. Liu, J. Am. Chem. Soc. 138 (2016) 36–39.
[29] C. Li, X.P. Han, F.Y. Cheng, Y.X. Hu, C.C. Chen, J. Chen, Nat. Commun. 6 (2015)

7345.
[30] M.A. Pena, J.L.G. Fierro, Chem. Rev. 101 (2001) 1981–2017.
[31] A. Grimaud, K.J. May, C.E. Carlton, Y.L. Lee, M. Risch, W.T. Hong, J.G. Zhou, Y. Shao-Horn, Nat. Commun. 4 (2013) 2439.
[32] J. Suntivich, K.J. May, H.A. Gasteiger, J.B. Goodenough, Y. Shao-Horn, Science 334 (2011) 1383–1385.
[33] F. Gao, X.Y. Chen, K.B. Yin, S. Dong, Z.F. Ren, F. Yuan, T. Yu, Z. Zou, J.M. Liu, Adv. Mater. 19 (2007) 2889–2892.
[34] O.P. Taran, A.B. Ayusheev, O.L. Ogorodnikova, I.P. Prosvirin, L.A. Isupova, V.N. Parmon, Appl. Catal. B 180 (2016) 86–93.
[35] C. Su, X. Duan, J. Miao, Y. Zhong, W. Zhou, S. Wang, Z. Shao, ACS Catal. 7 (2017) 388–397.
[36] C. Su, W. Wang, Y.B. Chen, G.M. Yang, X.M. Xu, M.O. Tade, Z.P. Shao, ACS Appl. Mater. Interfaces 7 (2015) 17663–17670.
[37] Y.M. Ren, L.Q. Lin, J. Ma, J. Yang, J. Feng, Z.J. Fan, Appl. Catal. B 165 (2015) 572–578.
[38] E. Saputra, S. Muhammad, H.Q. Sun, H.M. Ang, M.O. Tade, S.B. Wang, Environ. Sci. Technol. 47 (2013) 5882–5887.
[39] C.J. Liang, H.W. Su, Ind. Eng. Chem. Res. 48 (2009) 5558–5562.
[40] X.G. Duan, Z.M. Ao, L. Zhou, H.Q. Sun, G.X. Wang, S.B. Wang, Appl. Catal. B 188 (2016) 98–105.
[41] E.A. Betterton, M.R. Hoffmann, J. Phys. Chem. 92 (1988) 5962–5965.
[42] C.D. Qi, X.T. Liu, J. Ma, C.Y. Lin, X.W. Li, H.J. Zhang, Chemosphere 151 (2016) 280–288.
[43] Y.H. Guan, J. Ma, X.C. Li, J.Y. Fang, L.W. Chen, Environ. Sci. Technol. 45 (2011) 9308–9314.
[44] O.S. Furman, A.L. Teel, R.J. Watts, Environ. Sci. Technol. 44 (2010) 6423–6428.
[45] Y. Yang, J. Jiang, X.L. Lu, J. Ma, Y.Z. Liu, Environ. Sci. Technol. 49 (2015) 7330–7339.
[46] J. Ma, M.H. Sui, T. Zhang, C.Y. Guan, Water Res. 39 (2005) 779–786.
[47] Y.H. Guan, J. Ma, Y.M. Ren, Y.L. Liu, J.Y. Xiao, L.Q. Lin, C. Zhang, Water Res. 47 (2013) 5431–5438.
[48] H.W. Liang, H.Q. Sun, A. Patel, P. Shukla, Z.H. Zhu, S.B. Wang, Appl. Catal. B 127 (2012) 330–335.
[49] L.J. Xu, W. Chu, L. Gan, J. Chem. Eng. 263 (2015) 435–443.
[50] X.M. Xu, Y.B. Chen, W. Zhou, Z.H. Zhu, C. Su, M.L. Liu, Z.P. Shao, Adv. Mater. 28 (2016) 6442–6448.
[51] C. Norman, C. Leach, J. Membran. Sci. 382 (2011) 158–165.
[52] W. Zhou, M.W. Zhao, F.L. Liang, S.C. Smith, Z.H. Zhu, Mater. Horiz. 2 (2015) 495–501.
[53] X.G. Duan, C. Su, L. Zhou, H.Q. Sun, A. Suvorova, T. Odedairo, Z.H. Zhu, Z.P. Shao, S.B. Wang, Appl. Catal. B 194 (2016) 7–15.
[54] H.X. Li, J.Q. Wan, Y.W. Ma, Y. Wang, X. Chen, Z.Y. Guan, J. Hazard. Mater. 318 (2016) 154–163.
[55] Z.P. Shao, W.S. Yang, Y. Cong, H. Dong, J.H. Tong, G.X. Xiong, J. Membran. Sci. 172 (2000) 177–188.
[56] R.M. Navarro, M.C. Alvarez-Galvan, J.A. Villoria, I.D. Gonzalez-Jimenez, F. Rosa, J.L.G. Fierro, Appl. Catal. B 73 (2007) 247–258.
[57] X.P. Han, T.R. Zhang, J. Du, F.Y. Cheng, J. Chen, Chem. Sci. 4 (2013) 368–376.
[58] Z.P. Shao, S.M. Haile, Nature 431 (2004) 170–173.
[59] S. Baumann, F. Schulze-Kuppers, S. Roitsch, M. Betz, M. Zwick, E.M. Pfaff, W.A. Meulenberg, J. Membran. Sci. 359 (2010) 102–109.
[60] Z.P. Shao, S.M. Haile, J. Ahn, P.D. Ronney, Z.L. Zhan, S.A. Barnett, Nature 435 (2005) 795–798.
[61] J. Chen, Z. He, G. Li, T. An, H. Shi, Y. Li, Appl. Catal. B 209 (2017) 146–154.